Lab-scale measurements of wind farm blockage effects

Lab-scale measurements of wind farm blockage effects

Jan Bartl[1], Camilla H. Aasnæs[1], Joakim R. Bjørnsen[1], Gloria Stenfelt[1], David Lande-Sudall[1]

[1] Dept. of Mechanical and Marine Engineering, Western Norway University of Applied Sciences (HVL), 5063 Bergen, Norway

E-mail: jan.bartl@hvl.no

Abstract. The inflow an individual wind turbine experiences in a farm layout is strongly dependent on flow interaction effects with the turbines surrounding it. In addition to the well-known wake flows, lateral and upstream flow interaction effects, commonly described as wind farm blockage effects, have also recently gained some attention.
In this work, flow measurements in the upstream induction zone of neighboring turbines are presented for different arrangements of three to seven porous actuator discs. It is shown how the upstream induction zones of individual discs merge into a single zone when decreasing the lateral spacing between three discs. As a result, the central disc experiences a higher thrust force than its neighboring discs. For farm arrangements in two rows, an aligned disc setup is observed to result in a larger upstream velocity decrease than offset arrangements.

1. Introduction

The presence of a wind turbine rotor causes the upstream wind speed to reduce when approaching it. For an array of multiple neighboring turbines, this effect can increase as the induction zones of the single turbines can build up to a larger induction zone. While most of today's commercial wind farm flow models focus on wake effects only, these "wind farm blockage" or "induction zone" effects are not yet widely considered [1]. According to a recent study by Bleeg et al. [2], neglecting these effects has led to over-estimations of wind farm energy production. By combining power production field-data and flow simulations they showed that wind farm blockage led to lower front row power generation than expected for a single isolated wind turbine. An experimental and numerical investigation of the upstream induction zone of a single model wind turbine was presented by Medici et al. [3]. While experimental results showed a larger induction zone extension than predicted by vortex sheet theory, the numerical simulations gave a good match. Newer experimental results presented by Bastankhah & Porté-Agel [4] again show a good agreement of the upstream velocity field with vortex sheet theory.
A single row of wind turbines was investigated by Meyer Forsting et al. [5] using Computational fluid dynamics (CFD) simulations as well as an inviscid vortex model. Results show higher power production for the blocked central turbine compared to an isolated turbine. This power increase could be linked to a larger velocity reduction in the upstream induction zone when blocked by neighboring turbines. Power and flow field results from a tightly spaced row of three model wind turbines was presented by Feszty et al. [6]. The wind tunnel experiment found a larger induction zone for three turbines than an isolated turbine, and measured a higher power output for the central turbine. Wind tunnel experiments on larger model-scale wind farms were

presented by Ebenhoch et al. [7]. The tests indicated a much larger upstream induction zone when the farm's turbine density was increased. Their measurements and models showed that the inflow on a large wind farm can be affected up to 30 rotor diameters upstream from the first row. Segalini & Dahlberg [8] performed a combined experimental and numerical study, which indicated that the velocity decrease in the front row also depends on the wind farm layout. They proposed a simple functional dependency between the velocity decrease, number of rows and spacing. A large-eddy simulation by Wu & Porté-Agel [9] investigated flow effects inside and around large wind farms dependent on the stratification of the atmosphere. They found a significantly larger induction zone for stronger thermal stratification.
Drawing upon the analogous principles of operation, blockage effects and their impact on power production have also been studied for tidal stream turbines arranged in a channel of limited size. A model for tidal turbine power extraction dependent on channel blockage was developed by Garrett & Cummings [10]. Later, Nishino & Willden [11] introduced the idea of a global and local blockage for tidal turbines. They could derive an optimum lateral turbine spacing in a blocked channel. This concept was later applied to wind turbine rotors by Nishino & Draper [12]. They found that the limit of power extraction for a closely spaced lateral array of wind turbines increased when optimizing the local blockage.
In this paper we present lab-scale measurements of the upstream induction zone of three to seven turbines arranged in one and two rows. The basic turbine arrangements aim to give insight on how the upstream induction zone depends on turbine separation, an added second row and their configuration, whether offset or aligned. Compared to a real full-scale wind farm the presented experiments are intentionally performed with low spacing in order to better demonstrate the blockage effects. A number of additional experimental adaptions, such as a low number of turbines, no rotational effects and a rather high C_T present further simplifications compared to flow effects in full-scale wind farms.

2. Methods

2.1. Experimental setup

The model-scale experiments have been performed at the towing tank laboratory MarinLab at Høgskulen på Vestlandet (HVL) in Bergen, Norway. The towing tank has a total length of 50 m, a width of 3.0 m and a depth of 2.2 m. Figure 1 shows the experimental setup with an upside-down wind farm setup submerged in water. Performing aerodynamic experiments in water works well as both air and water are Newtonian fluids, i.e. they both follow the Reynolds scaling for incompressible flows. Aerodynamic experiments in water are thus not unusual and have been performed in both water flumes [13] as well as towing tanks [14], [15].
The single wind turbine rotors are represented by porous actuator discs with a solidity of $\sigma = 57$ % and a thrust coefficient of $C_T = 0.95$. The discs' geometry is shown in Figure 1, Detail 2b. The discs are manufactured from laser-cut aluminum and have a diameter of $D = 200$ mm and a thickness of $t = 5$ mm. The porosity is designed as radially increasing trapezoidal holes, which is similar to a number of actuator discs used in different wind tunnel experiments, e.g. Camp & Cal [16], Bossuyut et al. [17], Camp & Cal [18], de Jong Helvig et al. [19] or Neunaber et al. [20]. The design featuring a radially increasing local porosity is chosen to resemble the effective porosity of rotating blades. The center of each disc is screwed onto a small tower, which has a diameter of $D_{\text{Tower}} = 12$ mm and a total submerged length of $h = 300$ mm.

The whole setup is moved with a towing speed of $U_0 = 0.50$ m/ relative to still water, and the velocity field is measured by an *Vectrino+* Acoustic Doppler Velocimeter (ADV) produced by Nortek. The diameter-based Reynolds number in this experiment is $Re_D \approx 10^5$, which is about two orders of magnitude smaller than for a full-scale wind turbine, but comparable to most wind tunnel experiments with a post-critical flow regime which is assumed to be independent of

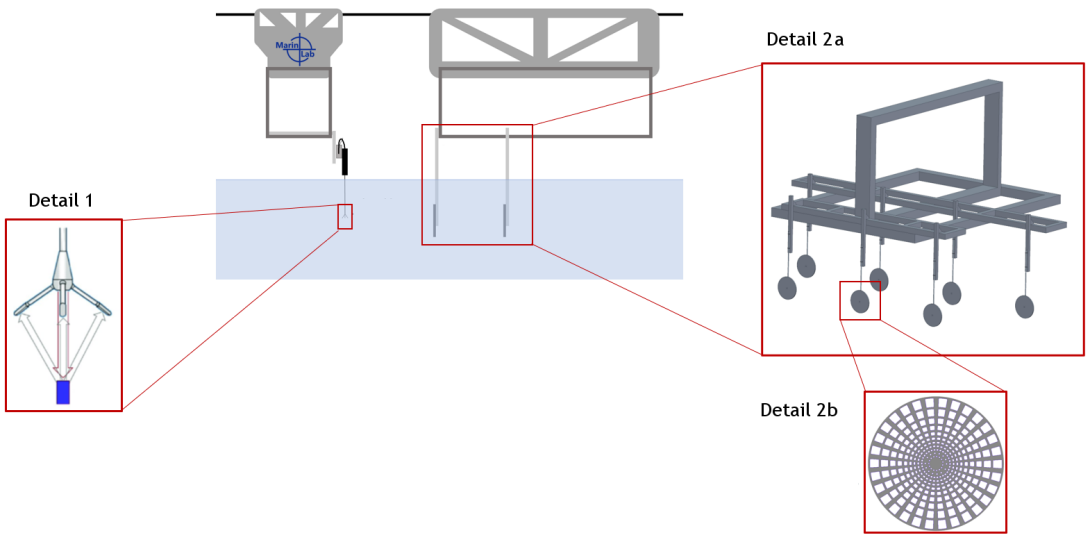

Figure 1. Sketch of the experimental setup: Towing carriages to which the ADV Vectrino+ is mounted (Detail 1) and the submerged setup of actuator discs (Detail 2a). Detail 2b shows the geometry of one porous disc.

Reynolds number. The ADV is mounted on to an automated traversing mechanism, enabling control of the horizontal position for the point measurements. As shown in Figure 1, Detail 1, the ADV's probe head was downwards facing. The probe was scanning the flow in a horizontal direction at a fixed depth $h = 300$ mm corresponding to the discs' center depth.

2.2. Flow measurements

The *Vectrino+* ADV is able to acquire all three velocity components at a sampling frequency of $f_{\text{sample}} = 200$ Hz. The instrument transmits a focused acoustic beam, which is reflected by seeding particles in a small volume that has a diameter of 6 mm and height of 3 mm. The back-scattered signal is registered by four receivers. The velocity vector is then calculated from the Doppler frequency, which makes it possible to acquire accurate velocity data without calibration. The ADV is equipped with a temperature sensor, which is used to calculate the temperature-dependent speed of sound in fresh water. The seeding particles are very small hollow neutrally-buoyant glass spheres with a mean diameter 10 μm. The effective towing length in the tank, where a constant, fully developed relative flow field is obtained, is about 25 m, which corresponds to a total sampling time of about 50s at a towing speed of $U_0 = 0.50$ m/s .

2.3. Test case overview

An overview over the different test cases is shown in Table 1. In a first set of experiments the lateral distance between the three front row turbines is varied from $s_y/D = 1.0$, 2.0 to 4.0 (disc center to disc center), i.e. at $s_y/D = 1.0$ the disc edges touch. In a second set, the first row is kept at a lateral separation of $s_y/D = 4.0$, while a second row is added at $s_x/D = 4.0$ downstream of it. These rather small turbine separations are only comparable to tightly spaced wind farms, e.g. Lillgrund wind farm [21], but were chosen intentionally in order to be able to see distinguishable effects. The number of discs in the second row was varied from two to four, in both aligned and offset setups. The measurement locations upstream of the front row for the wind farm (WF) setups is shown in Figure 2. Measurements have been taken along the upstream

Table 1. Test case overview: Single Disc (SD) and Wind Farm (WF) test cases.

Test case	**discs**	**rows**	s_y/D	s_x/D	**aligned/offset**
SD	1	1	-	-	-
WF3 1D	3	1	1	-	-
WF3 2D	3	1	2	-	-
WF3 4D	3	1	4	-	-
WF32 4D	5	2	4	4	offset
WF33 4D	6	2	4	4	aligned
WF34 4D	7	2	4	4	offset

centerline in negative x-direction in front of the central disc, outer disc and in between them. Transverse profiles have been taken in negative y-direction at $x/D = -0.4$ and $x/D = -1.0$.

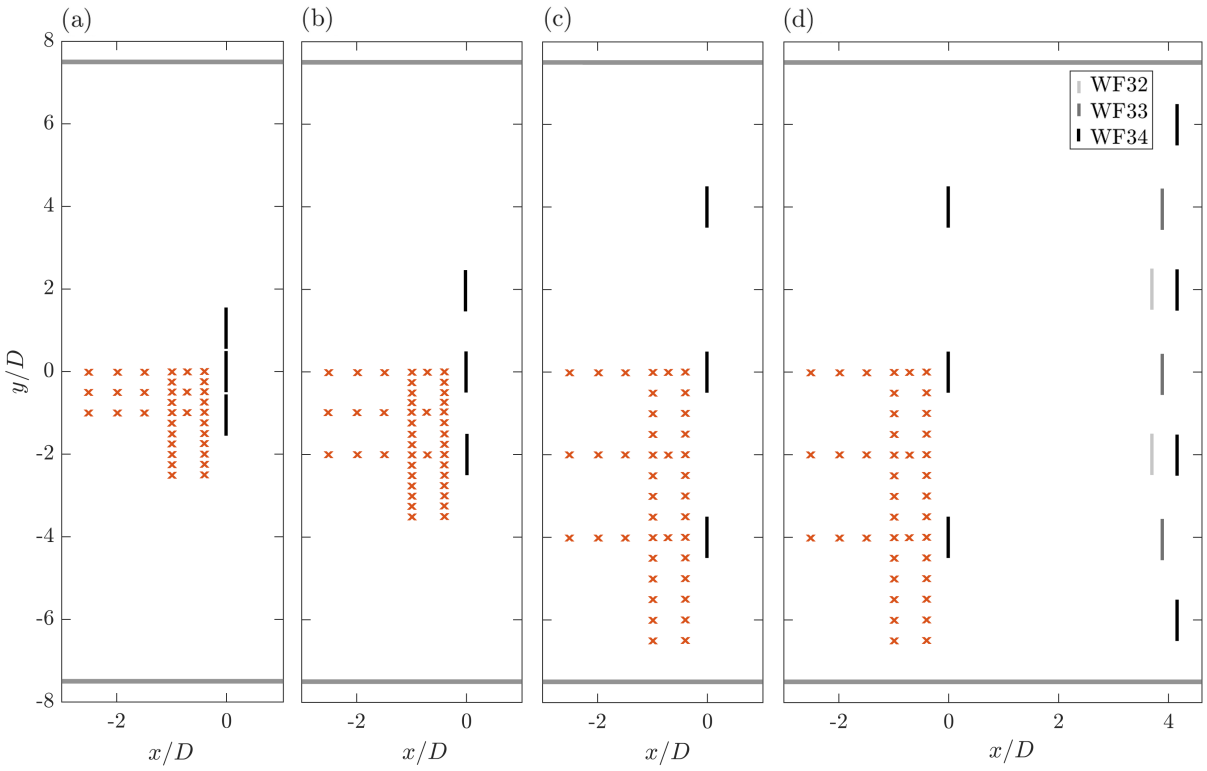

Figure 2. Measurement locations upstream of the different wind farm setups. (a) WF3 1D setup, (b) WF3 2D setup, (c) WF3 4D setup and (d) WF32, WF33 and WF34 setup. Red crosses (x) show measurement locations, gray horizontal lines indicate the towing tank walls (-).

3. Results

In this section, the results of the streamwise velocity in the upstream induction zone in front of the front row discs are presented and compared.

3.1. Single disc

Measurements of the velocity reduction along the centerline from $x/D = -3.0$ to $x/D = -0.4$ upstream of a single disc are shown in Figure 3 (a). The streamwise velocity is observed to be reduced to about 82% at half a rotor diameter upstream of the disc. The black line indicates the expected velocity decrease according to vortex sheet theory [4]:

$$\frac{U}{U_0} = 1 - a\left\{1 - \frac{2x}{D}\left[1 + \left(\frac{2x}{D}\right)^2\right]^{-\frac{1}{2}}\right\} \tag{1}$$

where a is the axial induction factor of the rotor or disc. The axial induction factor is estimated from the measured C_T coefficient, according to the one-dimensional momentum theory for ideal rotors [22]:

$$a = \frac{1}{2} - \frac{1}{2}(1 - C_T)^{\frac{1}{2}} \tag{2}$$

The measured velocity is observed to decrease further upstream than predicted by vortex sheet theory, but generally it follows its trend very well. A possible explanation for this slight mismatch is a radial variation in induction factor a and thrust coefficient C_T that is not taken into account in the simplified equations (1) and (2). Figure 3 (b) shows a transverse profile measured at $x/D = -1.0$ upstream of a single disc, where a maximum velocity decrease to 95.5% of the incoming velocity is measured upstream of the center. The velocity profile follows a Gaussian shape, and is seen to have a relative velocity $U/U_0 > 1$ for $y/D >| 1 |$ indicating flow acceleration around the disc. The errorbars indicate the precision error calculated from the standard deviation from repeated measurements in one half of the induction zone.

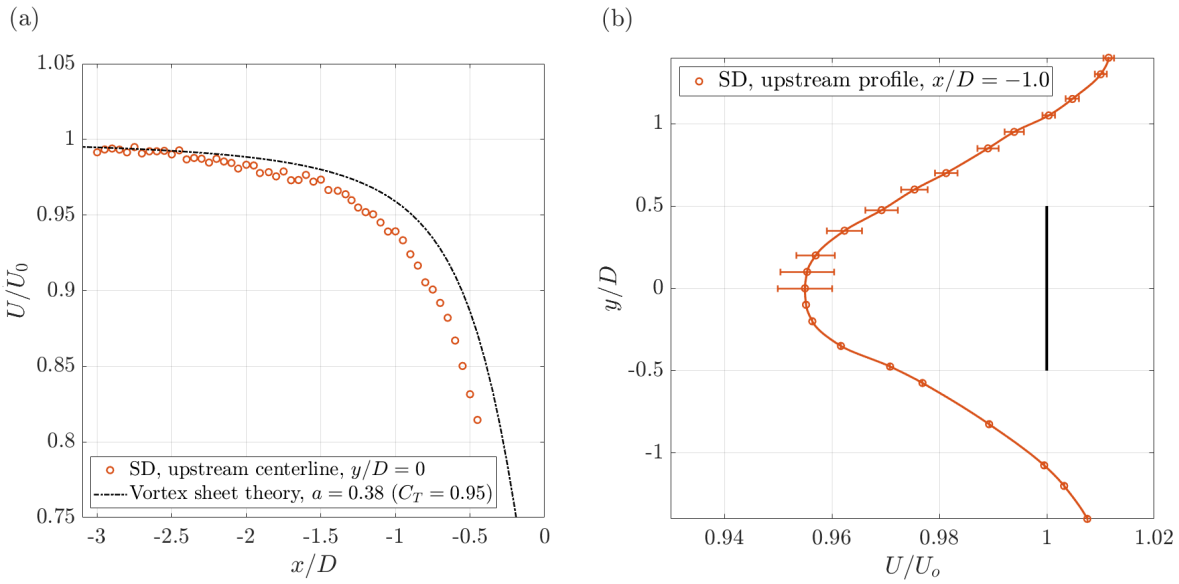

Figure 3. Upstream induction zone for a single disc (SD). (a) Upstream centerline at $y/D = 0$ compared to theory and (b) Upstream horizontal profile at $x/D = -1.0$

3.2. One-row wind farm

In the first set of experiments the lateral influence on the induction zone of a central disc from two neighboring discs is investigated. As shown in Figure 4, three different lateral separation distances are tested, (a) $s_y/D = 1$, (b) $s_y/D = 2$ and (c) $s_y/D = 4$. Horizontal velocity profiles are measured at x/D=-0.4 and x/D=-1.0 upstream of the front row.

For the closest disc separation $s_y/D = 1$, the induction zones of the individual discs clearly have merged into one single induction zone. At x/D=-1.0 the relative velocity decreases to 88% in front of the central disc. The horizontal profile has a Gaussian shape at this location, indicating that the flow here sees one large object rather than three individual discs. Closer to the setup, at x/D=-0.4, distinct peaks in the disc centers are clearly distinguishable, yet the individual zones have clearly merged. A larger maximum relative velocity reduction of 71% upstream of the central disc is measured here, indicating significant blockage of the neighboring discs.

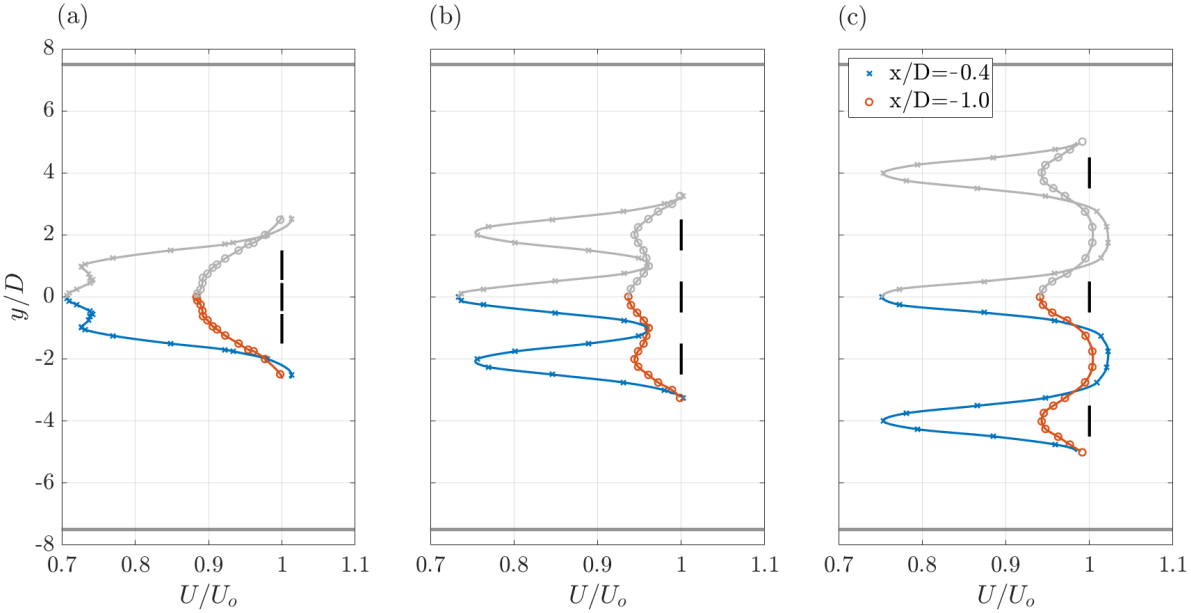

Figure 4. Horizontal velocity profiles measured at x/D=-0.4 and x/D=-1.0 in the upstream induction zone for WF3. The lateral separation of the three discs is (a) $s_y/D = 1$, (b) $s_y/D = 2$ and (c) $s_y/D = 4$. Gray colored lines indicate mirrored data for the symmetrical setup.

When increasing the lateral disc separation to $s_y/D = 2$, as shown in Figure 4 (b), both velocity profiles at x/D=-0.4 and -1.0 show three distinct peaks. The higher velocity reduction upstream of the central disc indicates a higher local blockage. A maximum reduction in relative velocity of 74% is measured at x/D=-0.4. When the lateral disc separation is furthermore increased to $s_y/D = 4$ (Figure 4 (c)), the flow profiles measured at both upstream distances are very similar in front of the individual discs. The maximum decrease in relative velocity at x/D=-0.4 is measured at 76% for both the central and outer discs. A significant flow acceleration is observed in the zone in-between the disc, clearly separating the individual induction zones from each other.

3.3. Two-row wind farm

In the second setup, the lateral separation between the front row discs is kept constant at $s_y/D = 4$, while a second row of two offset (WF32), three aligned (WF33) and four offset (WF34) discs is added at $s_x/D = 4$ disc diameters downstream. The upstream flow is measured at the same locations as earlier. The mean normalized velocity field of the streamwise component are compared for the three setups in Figure 5.

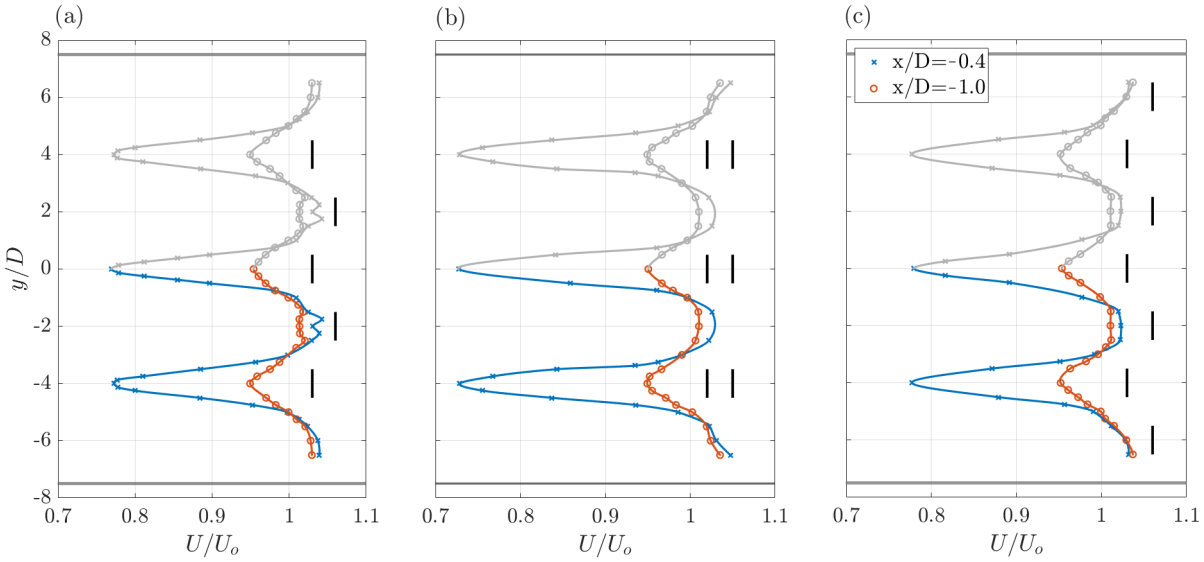

Figure 5. Horizontal profiles of the mean streamwise velocity component measured at x/D=-0.4 and x/D=-1.0 measured in the upstream induction zone for (a) WF32, (b) WF33 and (c) WF34. Grey colored lines indicate mirrored data for the symmetrical setup.

It is observed that the relative upstream velocity reduction for the offset cases, WF32 and WF34, is similar to that of the single row farm, WF3. The offset row of downstream turbines is seen to influence the velocity profiles only in-between the front row discs, while the peak levels in velocity reduction are not influenced. Furthermore, the peak levels at x/D=-0.4 and -1.0 do not vary much between the central and outer front row disc, indicating that the additional blockage imposed from the downstream discs is not significant. This observation is somewhat expected, given that the upstream influence of a disc s_x/D=4 downstream is expected to be minimal according to vortex sheet theory previously shown in Figure 3.
However, considerably larger upstream velocity reductions are measured for the WF33 case. Here, three aligned downstream discs are seen to induce relative velocity reductions down to 72% at x/D=-0.4, in front of both the central and outer disc in the front row.

3.4. Comparison of different setups

The upstream velocity reduction in front of the central front row disc measured at x/D=-1.0 is compared for all the different setups in Figure 6.

The most significant effects on the upstream velocity are observed for a tight lateral disc spacing as depicted in Figure 6 (a). As mentioned in the introduction, such small lateral separations between s_y/D=1-2 are rather unrealistic in normal wind farm arrangements. For tightly-spaced multirotor arrangements as described in [23],[24], however, such small rotor separations could be relevant. For the largest lateral separation, s_y/D=4 investigated here, the velocity profile is observed to be very similar to that measured upstream of a single disc (SD). The local blockage of the central disc has become so small, that the upstream velocity

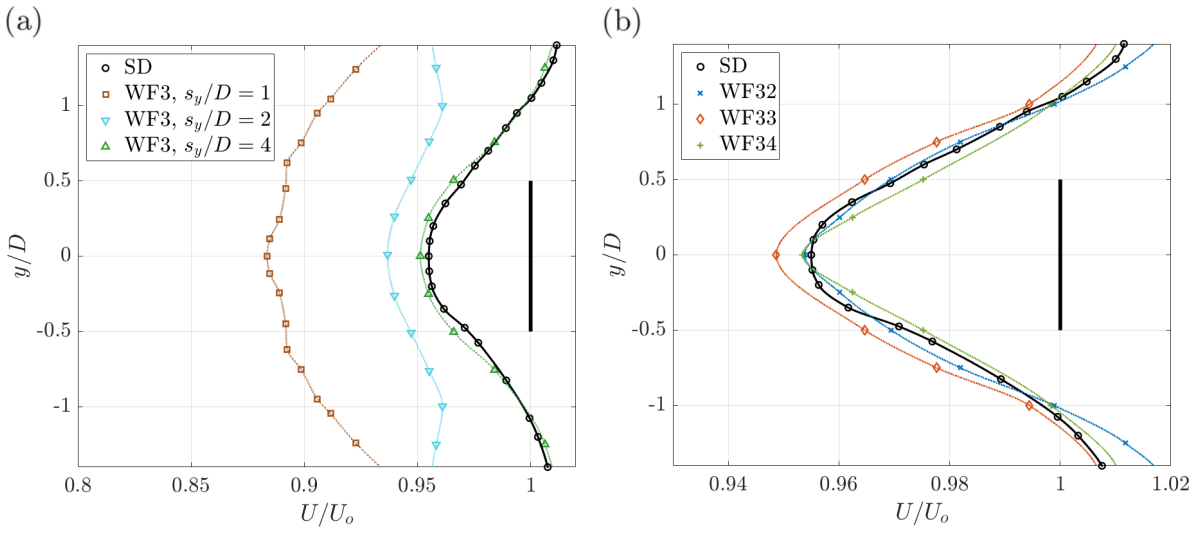

Figure 6. Comparison of upstream velocity profile at x/D=-1.0 upstream of central disc for (a) SD vs. WF3 for different lateral separations s_y/D and (b) SD vs. WF32, WF33 and WF34.

profile at x/D=-1.0 is not significantly affected.
The upstream velocity profile at x/D=-1.0 for arrangements of a tightly spaced, two-rowed wind farm with an inter-turbine spacing of s_x/D=s_y/D=4 is compared in Figure 6 (b). While the upstream flow field is unaltered for offset setups WF32 and WF34, the aligned WF33 setup shows an additional small deceleration of the incoming flow upstream of the front row. These results indicate that the turbine arrangement in a farm setup, relative to the incoming wind direction might play an important role for wind farm blockage effects. However, it is at this point not clear, how a larger number of turbines and downstream rows affect the upstream induction zone.

4. Conclusions and Future Work

Flow measurements in the upstream induction zone of small wind farm setups have been presented. For one row of three turbines an additional decrease in the relative velocity upstream of the central turbine could be observed when the lateral distance to its neighboring turbines was decreased. For higher lateral separations $s_y/D \geq 4$, however, no significant influence on the induction zone of the center disc is determined. When adding a second row of discs at four rotor diameters downstream, a significantly higher upstream velocity reduction is assessed for a set of aligned downstream discs. For an offset second row, however, the induction zone upstream of the front row remains unchanged. These results confirm the findings from Segalini & Dahlberg [8], where upstream velocity reductions for up to two rows are minimal.
Future work will therefore also investigate these effects for a larger number of turbine rows and a larger total blockage. Force measurement on the individual discs will also be provided. Additional wake measurements will examine how the upstream induction zone is influenced by the expansion and merging of the single turbines' wake into a wind farm wake downstream. Furthermore, the experimental results will be complemented by a numerical simulation framework including both high-fidelity Detached-Eddy-Simulations (DES) as well as low-fidelity flow-superposition modeling.

Acknowledgments
The authors thank the lab engineers at HVL, Nafez Ardestani, Kjetil Gravelsæter, Frode W Jansen, Robert Larsson, Bernt H Hembre and Harald Moen for constructing the traversing mechanism and support during the experiments.

References

[1] Branlard E and Meyer Forsting A R 2020 *Wind Energy* **23** 2068–2086
[2] Bleeg J, Purcell M, Ruisi R and Traiger E 2018 *Energies* **11** 1609
[3] Medici D, Ivanell S, Dahlberg J Å and Alfredsson P H 2011 *Wind Energy* **14** 691 – 697
[4] Bastankhah M and Porté-Agel F 2017 *Phys. Fluids* **29** 065105
[5] Meyer Forsting A R, Troldborg N and Gaunaa M 2017 *Wind Energy* **20** 63–77
[6] Feszty D, McTavish S, Bodnya I and Jee D 2016 *AIAA* **2016-4820**
[7] Ebenhoch R, Muro B, Dahlberg J, Hägglund P and Segalini A 2016 *Wind Energy* **20** 859–875
[8] Segalini A and Dahlberg J 2020 *Wind Energy* **23** 120–128
[9] Wu K and Porté-Agel F 2017 *Energies* **10** 2164
[10] Garrett C and Cummins P 2007 *J. Fluid Mech.* **588** 243 – 251
[11] Nishino T and Willden R 2012 *J. Fluid Mech.* **708** 596–606
[12] Nishino T and Draper S 2015 *J. Phys.: Conf. Ser.* **625** 012010
[13] Okulov V, Mikkelsen R, Sørensen J, Naumov I and Tsoy M 2017 *J. Energ. Resour.-ASME* **139** 051210–2
[14] Barber S, Wang Y, Jafari S, Chokani N and Abhari R 2011 *J. Sol. Energy Eng.* **133** 011007
[15] Kress C, Chokani N and Abhari R 2016 *Renew. Energ.* **89** 543–551
[16] Camp E and Cal R 2016 *Phys. Rev. Fluid.* **1** 044404
[17] Bossuyt J, Howland M, Meneveau C and Meyers J 2017 *Exp. Fluid* **58**
[18] Camp E and Cal R 2019 *Phys. Rev. Fluid.* **4** 024610
[19] Helvig S d J, Vinnes M K, Segalini A, Worth N A and Hearst R J 2021 *J. Wind Eng. Ind. Aerod.* **209** 104485
[20] Neunaber I, Hölling M, Whale J and Peinke J 2021 *Renew. Energ.* **179** 1650–1662
[21] Nilsson K, Ivanell S, Hansen K, Mikkelsen R, Sørensen J, Breton S and Henningson D 2015 *Wind Energy* **18** 449–467
[22] Hansen M 2008 *Aerodynamics of Wind Turbines* 2nd ed (Earthscan) ISBN 978-1-84407-438-9
[23] vdLaan P, Andersen S, García N, Angelou N, Pirrung G, Ott S, Sjöholm M, Sørensen K, Neto J, Kelly M, Mikkelsen T and Larsen G 2019 *Wind Energ. Sci.* **4** 251–271
[24] Bastankhah M and Abkar M 2019 *Phys. Fluids* **31** 085106